Propulsion and Power Research 2015;4(2):72–83

HOSTED BY

ELSEVIER

http://ppr.buaa.edu.cn/

Propulsion and Power Research

www.sciencedirect.com

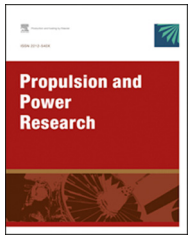

Characteristics of transonic moist air flows around butterfly valves with spontaneous condensation

A.B.M. Toufique Hasan[a,*], S. Matsuo[b], T. Setoguchi[b]

[a]*Department of Mechanical Engineering, Bangladesh University of Engineering and Technology (BUET), Dhaka-1000, Bangladesh*
[b]*Department of Advanced Technology Fusion, Saga University, Saga 8408502, Japan*

Received 10 November 2013; accepted 29 April 2015
Available online 26 June 2015

KEYWORDS

Transonic flow;
Shock waves;
Spontaneous condensation;
Butterfly valves;
Reynolds-averaged Navier-Stokes (RANS)

Abstract Effects of spontaneous condensation of moist air on the shock wave dynamics around butterfly valves in transonic flows are investigated by experimental and numerical simulations. Two symmetric valve disk shapes namely- a flat rectangular plate and a mid-plane cross-section of a prototype butterfly valve have been studied in the present research. Results showed that in case with spontaneous condensation, the root mean square of pressure oscillation (induced by shock dynamics) is reduced significantly with those without condensation for both shapes of the valves. Moreover, local aerodynamic moments were reduced in case with condensation which is considered to be beneficial in torque requirement in case of on/off applications of valves as flow control devices. However, total pressure loss was increased with spontaneous condensation in both the valves. Furthermore, the disk shape of a prototype butterfly valve showed better aerodynamic performances compared to flat rectangular plate profile in respect of total pressure loss and vortex shedding frequency in the wake region.

1. Introduction

Investigation on the aerodynamic characteristics of butterfly valves has been performed for the last many years due to their technological and industrial importance. This type of valves are used intensively in aircraft outflow valves to regulate the cabin pressure in pressurized aircraft [1], in hydro-electric power schemes as safety valves [2] as well as in nuclear containment

*Corresponding author. Tel.: +(880) 1730714444.
E-mail address: toufiquehasan@me.buet.ac.bd (A.B.M. Toufique Hasan).
Peer review under responsibility of National Laboratory for Aeronautics and Astronautics, China.

http://dx.doi.org/10.1016/j.jppr.2015.05.003

Nomenclature

c	chord length of butterfly valve (unit: mm)
f	frequency of shock oscillation (unit: kHz)
g	condensate mass fraction (unit: -)
H	height of the channel (unit: mm)
I	nucleation rate (unit: $1/(m^3 \cdot s)$)
k	turbulent kinetic energy (unit: m^2/s^2)
Ma	Mach number (unit: -)
p	static pressure (unit: kPa)
R	undamped eddy viscosity (unit: m^2/s)
Re	Reynolds number (unit: -)
S	degree of supersaturation (unit: -)
RMS	root mean square (unit: -)
x	streamwise coordinate (unit: mm)
y	normal coordinate (unit: mm)
T	time period (unit: s) / temperature (unit: K)
t	time (unit: s) / thickness (unit: mm)

Greek symbols

β	integrated total pressure loss (unit: -)
θ	angle of attack (unit: °)

Subscripts

ave	average
b	back pressure
l	lower surface
u	upper surface
0	upstream condition
0l	total/stagnation condition at inlet

purge valves as flow controllers [3,4] and so on. Butterfly valve disks behave in the same manner as airfoils that the angle of attack influences the flow field characteristics [5]. However, under a certain combination of valve disk opening angle and pressure difference across the valve, compressible flow effects can significantly alter the performance characteristics and flow field of a butterfly valve [6]. At these conditions, regions of transonic and supersonic flow can develop in the vicinity of the valve disk and downstream of it. Morris and Dutton [7] experimentally studies the flow field and torque of a compressible fluid in a butterfly valve. The 2-D experimental investigations were performed over a range of disk positions and pressure ratios. Recently, butterfly valve performance coefficients (such as lift, drag, resultant force and torque coefficients) in compressible flow field were predicted using computational fluid dynamics (CFD) [4]. However, in transonic or supersonic flow field, expansion of vapor/carrier gas mixture (moist air) or steam is often so rapid that the flow field gives rise to spontaneous (homogeneous and non-equilibrium) condensation process [8,9]. In this process, first the vapor molecules itself generate condensation nuclei spontaneously by molecular collision, and secondly, the condensation of the vapor molecules take place on these nuclei (droplet growth). This condensation process releases thermal energy to the surrounding gaseous medium and considerably modifies their thermo-fluid behaviors. This phenomena is evident by the presence of water droplet which was seen in the exhaust plume during the experimental testing performed by Leutwyler and Danban [4] and responsible for the difference between previous numerical and experimental results. Thus, to predict accurately the flow field around butterfly valve in compressible flows, working fluid must need to be considered as multiphase fluid.

In the present study, the effect of moist air with the occurrences of spontaneous homogeneous condensation on transonic internal flow around a symmetric disk butterfly valve is investigated. Two valve disk shapes have been studied in the present study: a flat rectangular plate profile and a mid-plane cross-section of a prototype butterfly valve. Results are presented for various aerodynamic aspects for the case of moist air. Further the results are compared with those of no condensation of dry air.

2. Numerical methods

2.1. Governing equations

The transonic flow through the symmetric disk butterfly valves is governed by the unsteady compressible Navier-Stokes equations written in two-dimensional coordinate system (x, y). To link the heat supply by condensation process, a rate equation of liquid-phase production [10] was coupled. As a turbulence model, a modified two-equation k-R model [11,12] was used in the present computation where k and R are the turbulent kinetic energy and the undamped eddy viscosity, respectively. These equations were discretized by the finite difference technique. A third order TVD (total variation diminishing) finite difference scheme with MUSCL [13] was employed to discretize the spatial derivative, and a second order central difference scheme for viscous terms, and a second order fractional step method was used for time integration. For simplicity of the computation, assumptions are as follows; no velocity slip and no temperature difference between condensate particles and gas medium, and the effect of condensate particles on pressure is negligible.

Figure 1 shows the computational domain of the flow field, details of test section and two different valve geometries (rectangular plate and mid-plane cross-section of a prototype butterfly valve). The prototype butterfly valve is similar to that used in previous study [3]. Chord length, c and the thickness of the valve, t are 48 mm and 7.2 mm (aspect ratio: $t/c = 0.15$), respectively. The height of the test section H is 60 mm ($H/c = 1.25$). Angle of attack of the valve is denoted by θ; where θ is the angle between x-axis (reference axis) and the line joining the leading and trailing edges of the valve (Figure 1(c)). Computational domain is

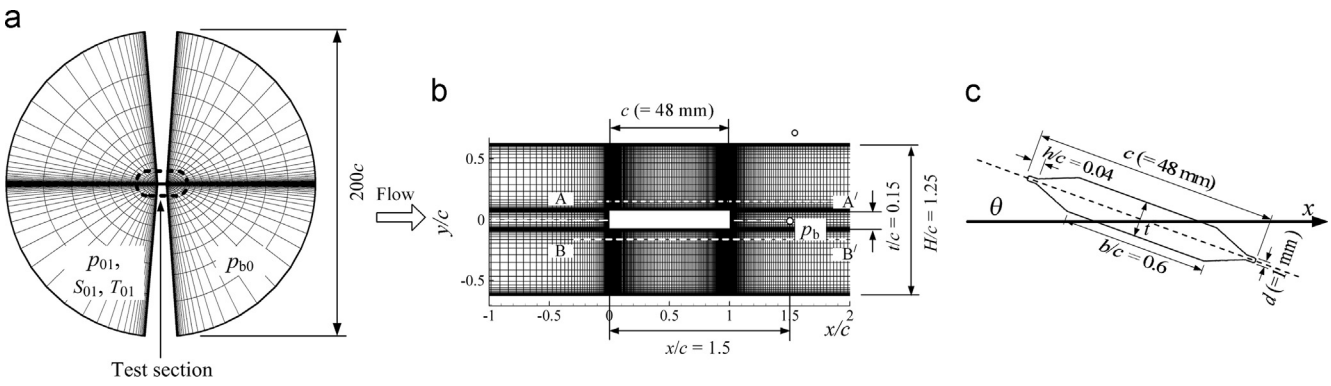

Figure 1 Computational domain, test section and valve geometries. (a) Computational domain, (b) details of test section with a rectangular plate, and (c) prototype butterfly valve with θ.

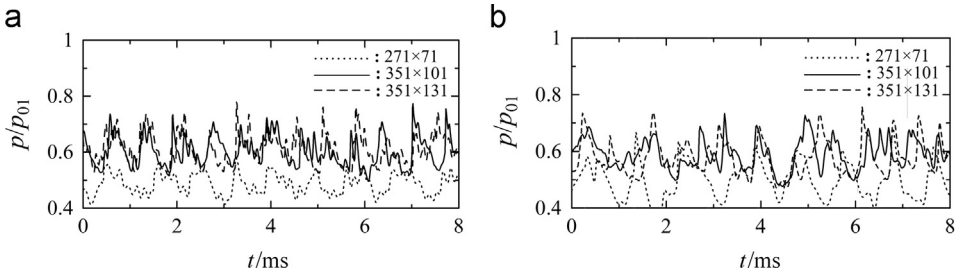

Figure 2 Time histories of static pressure at $x/c=0.83$, and $y/c=0.31$ for $S_{01}=0$. (a) $\theta=0^\circ$ and (b) $\theta=3.2^\circ$.

discretized by structured mesh. The origin of (x, y) coordinate is located at leading edge of the valve. Aerodynamic and condensate properties are measured along line A-A' and B-B' which are vertically $0.075c$ apart from the valve upper and lower surfaces, respectively.

Working gas used in the present study is moist air which is assumed to be thermally and calorically perfect. Inlet Mach number, Ma upstream of the valve is 0.6 and Reynolds number based on valve chord length is 5.4×10^5. The pressure ratio p_{b0}/p_{01} (p_{b0}: total back pressure, p_{01}: reservoir total pressure) was kept at 0.739 [14]. Values of initial degree of supersaturation, S_{01} are 0 for dry air and 0.6 for moist air. Total temperature, T_{01} and total pressure, p_{01} in the reservoir are 298.15 K and 101.3 kPa, respectively.

Inlet boundary was fixed, and exit boundary was constrained with free boundary condition. Non-slip and adiabatic wall conditions were applied at the solid boundary. The pressure at the wall was obtained from zero normal pressure gradient on the body surface. Condensate mass fraction g was set to zero on the solid wall.

3. Results and discussion

Figures 2(a) and (b) show numerical results of time variations of static pressures in case of prototype valve at $x/c=0.83$, $y/c=0.31$ for $\theta=0^\circ$ and $\theta=3.2^\circ$, respectively, for $S_{01}=0$. The ordinate designates the static pressure ratio and the abscissa the elapsed time in ms. Dotted lines show numerical results obtained with coarse meshes of 271×71. Solid and dashed lines show those with fine meshes of 351×101 and 351×131, respectively. The results obtained with fine meshes show relatively similar fluctuation but one obtained with the coarse mesh shows a significant difference in amplitude. This implies the numerical result varies significantly depending on the mesh sizes. However, the trend obtained by these finer mesh simulation only show nearly identical fluctuation in amplitude and a slight discrepancy in phase. Hence, in this study finer mesh size is used.

It was found that the oscillation frequency (in dry air) varied significantly depending on the mesh size. However, for finer mesh sizes, the calculated frequency in case of $\theta=0^\circ$ was 1.224 kHz compared to experimental data (using a pressure transducer: Toyoda model PMS-5 500 K with resonance frequency of 40 kHz) of 1.216 kHz. In the flow case of $\theta=3.2^\circ$, the computed frequency deviates within 0.8% compared to the experiments. Moreover, computed frequencies using finer mesh agreed well with experimental data in case with spontaneous condensation. Thus, a mesh size of 351×101 was adopted for all the numerical computations in the present study.

Now the flow structure in transonic flows around symmetric disks will be discussed. Figures 3(a) and (b) show instantaneous schlieren photographs around a plate in cases without and with spontaneous condensation by experiments, respectively ($\theta=3.2^\circ$). The detail experimental setup are not shown here for brevity and can be found in Ref. [15]. Since there were no shock waves, results for $\theta=0^\circ$, are not shown

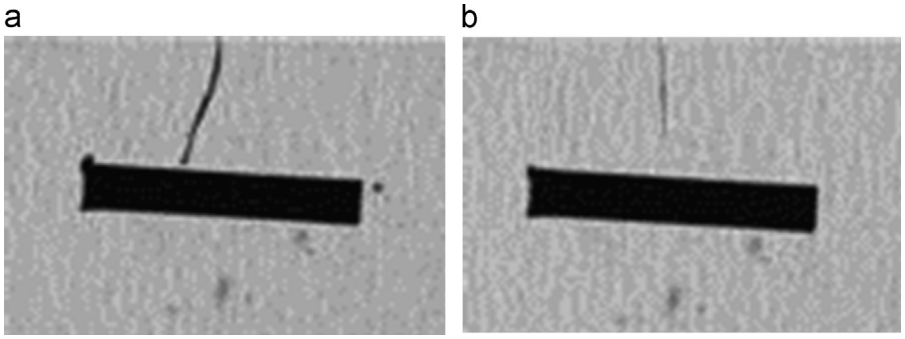

Figure 3 Schlieren photographs (plate, $\theta=3.2^\circ$). (a) $S_{01}=0.17$ and (b) $S_{01}=0.60$.

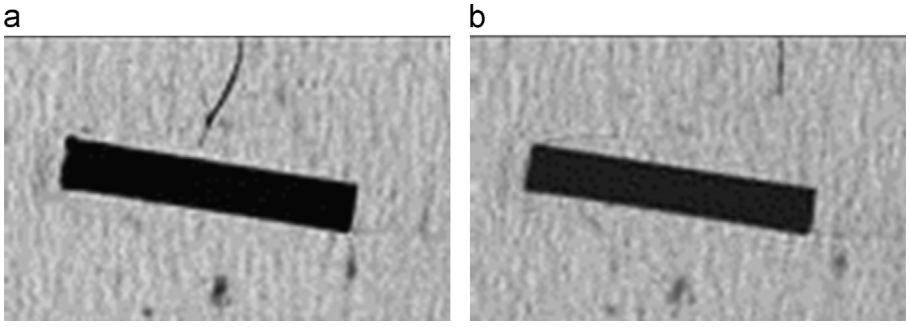

Figure 4 Schlieren photographs (plate, $\theta=8.5^\circ$). (a) $S_{01}=0.17$ and (b) $S_{01}=0.60$.

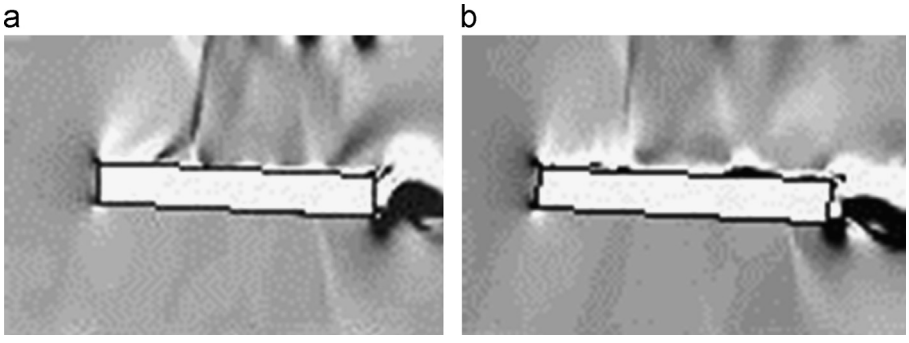

Figure 5 Computer numerical schlieren (plate, $\theta=3.2^\circ$). (a) $S_{01}=0$ and (b) $S_{01}=0.60$.

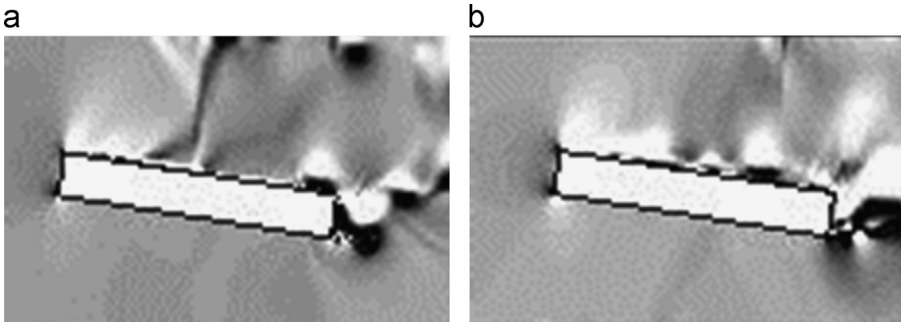

Figure 6 Computer numerical schlieren (plate, $\theta=8.5^\circ$). (a) $S_{01}=0$ and (b) $S_{01}=0.60$.

here. Figure 4 show instantaneous schlieren photographs for $\theta=8.5^\circ$. In the experimental facilities, the atmospheric air can be dehumidified upto $S_{01}=0.17$ and the results are shown in Figures 3(a) and 4(a). In this case, the degree of supersaturation is so small that the air can be considered to be almost dry [16]. Ranges of shock oscillation in the upper passage of plate for $\theta=3.2^\circ$ and $\theta=8.5^\circ$ are $x/c=0.2$ to $x/c=0.5$ and $x/c=0.45$ to $x/c=1.0$, respectively in this case.

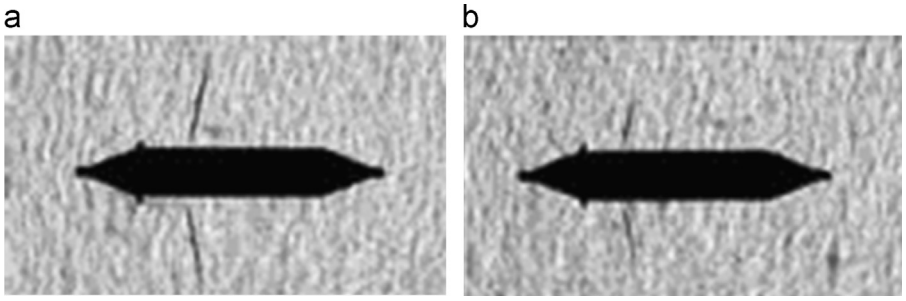

Figure 7 Schlieren photographs (prototype butterfly valve, $\theta=0^\circ$). (a) $S_{01}=0.17$ and (b) $S_{01}=0.60$.

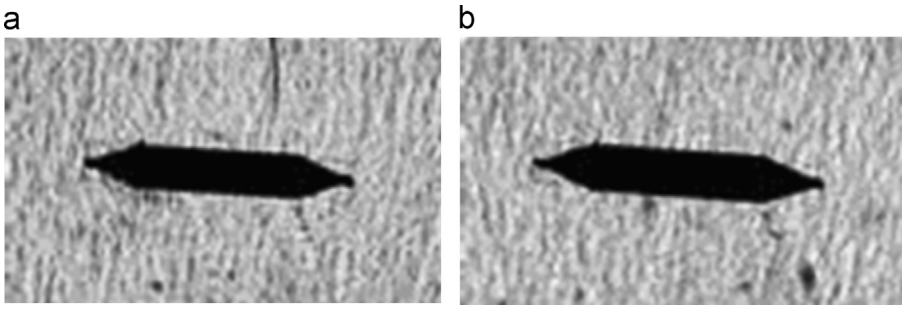

Figure 8 Schlieren photographs (prototype butterfly valve, $\theta=3.2^\circ$). (a) $S_{01}=0.17$ and (b) $S_{01}=0.60$.

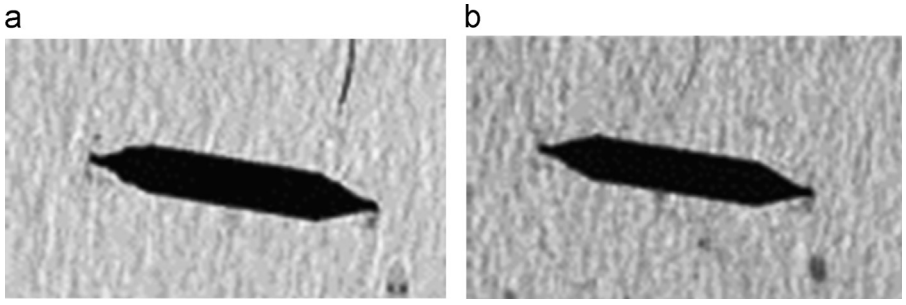

Figure 9 Schlieren photographs (prototype butterfly valve, $\theta=8.5^\circ$). (a) $S_{01}=0.17$ and (b) $S_{01}=0.60$.

However, in case with spontaneous condensation (Figures 3 (b) and 4(b)), it seems that the configuration of the shock wave changes largely and its strength becomes weaker compared to those in Figures 3(a) and 4(a). Figures 5 and 6 show computer generated schlieren pictures (density gradient) corresponding to each figure in Figures 2 and 3, respectively. The flow structures obtained by simulation are agreed well with experimental results.

In case of a prototype butterfly valve, instantaneous schlieren photographs for the cases of without and with spontaneous condensation by experiments are shown in Figures 7(a) and (b), respectively ($\theta=0^\circ$). Figures 8 and 9 show instantaneous experimental schlieren photographs for $\theta=3.2^\circ$ and $\theta=8.5^\circ$, respectively. In these cases, the spontaneous condensation also changes the shock structure and the shock strength becomes weaker to that of dry air case as discussed for plate. However, in case of $S_{01}=0.60$, the shock wave moves further upstream to that of dry air for $\theta=3.2^\circ$ and $\theta=8.5^\circ$. The upstream movement of the shock waves is due to the reduction of degree of flow expansion (thus the reduction of upstream shock Mach number) which is induced by the addition of heat to the supersonic flow field through spontaneous condensation in case of moist air. Figures 10–12 show computer generated schlieren pictures (density gradient) corresponding to each figure in Figures 7–9, respectively. As seen from these figures, the flow structures obtained by simulation are similar to experimental results. However, a slight difference of numerical shock structure from experimental one is observable, which is obviously created due to the complexities in real flows, the main flow non-uniformity and the sidewall boundary layers, which are never taken into account in usual 2-D numerical simulations.

Figure 13 shows distributions of static pressure p/p_{01}, nucleation rate I and condensate mass fraction g along the line A-A' during one cycle of flow oscillation for $\theta=0^\circ$ around a plate. T is a period of one cycle of flow oscillation measured at $x/c=1.5$, $y/c=0$ (will be discussed latter). In case of $S_{01}=0$, it is found that weak compression wave is generated at the position close to the plate trailing edge. For $S_{01}=0.6$, this compression wave is weaken by the development of nucleation zone in the range of $x/c \approx 0.9 \sim 1.1$ which causes the generation

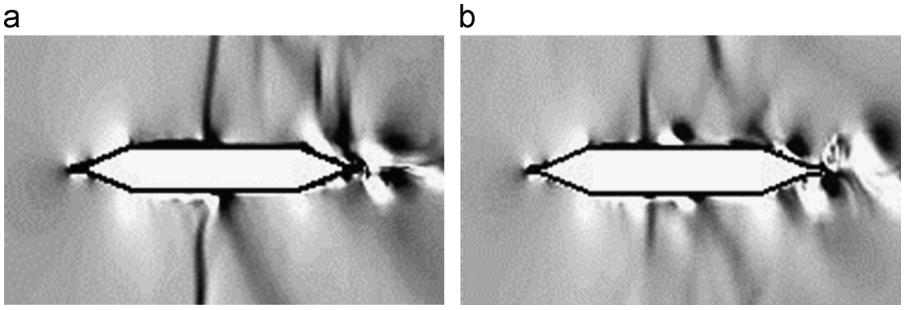

Figure 10 Computer numerical schlieren (prototype butterfly valve, $\theta=0^\circ$). (a) $S_{01}=0$ and (b) $S_{01}=0.60$.

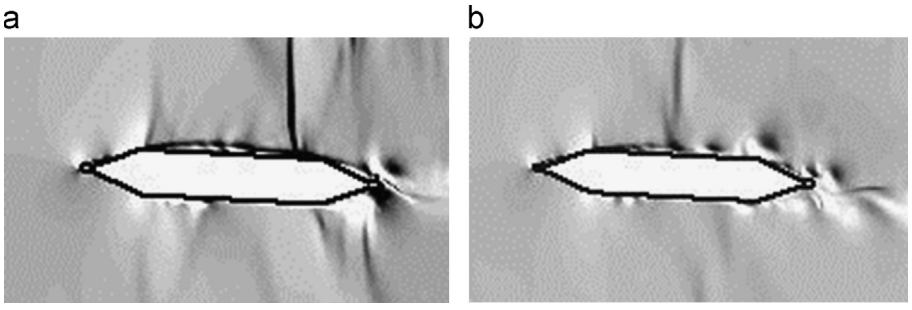

Figure 11 Computer numerical schlieren (prototype butterfly valve, $\theta=3.2^\circ$). (a) $S_{01}=0$ and (b) $S_{01}=0.60$.

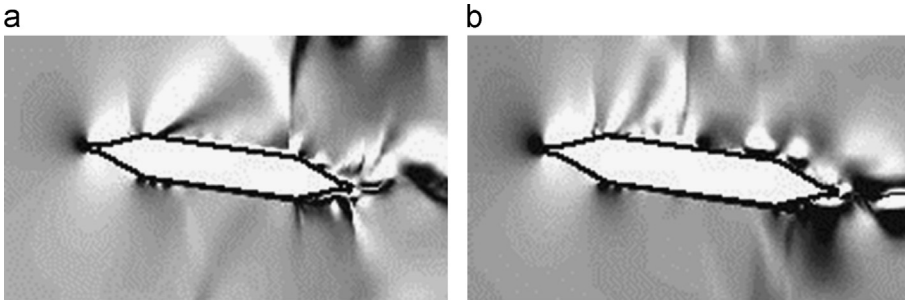

Figure 12 Computer numerical schlieren (prototype butterfly valve, $\theta=8.5^\circ$). (a) $S_{01}=0$ and (b) $S_{01}=0.60$.

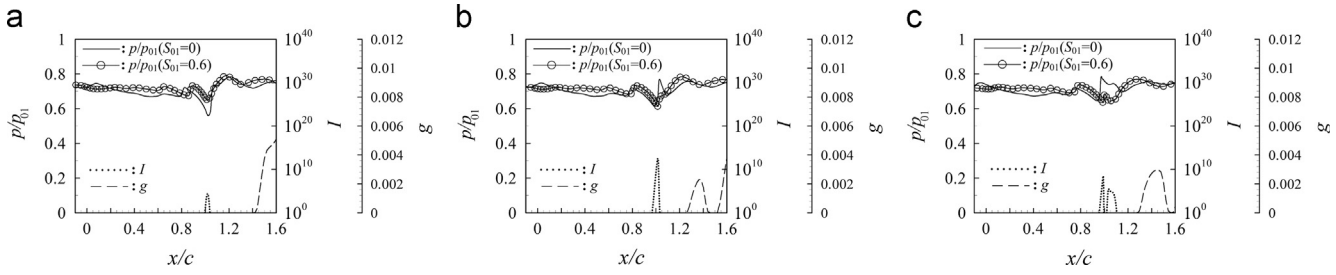

Figure 13 Distributions of static pressure (p/p_{01}), nucleation rate (I) and condensate mass fraction (g) along line A-A' around a plate ($\theta=0^\circ$). (a) $t=0.333T$ (ms), (b) $t=0.667T$ (ms), and (c) $t=1.000T$ (ms).

of condensate particles downstream of the plate. For $\theta=3.2^\circ$, strong shock wave is generated around the plate upper surface in the range of $x/c\approx0.20\sim0.50$ for $S_{01}=0$ as shown in Figure 14. In case of the occurrence of spontaneous condensation ($S_{01}=0.6$), development of a nucleation zone is observed due to rapid flow expansion in the region close to the plate leading edge, and nucleation rate I reaches the peak value where static pressure falls to a minimum and then decreases rapidly after the maximum. Condensate mass fraction begins to increase from the position where nucleation rate reaches the peak and after that, varies further downstream of the position. The maximum of g values is about 0.006 along line A-A' for $\theta=3.2^\circ$ ($S_{01}=0.6$). The reduction of shock strength is considered to be due to reduction of Mach number upstream of the shock by the generation of liquid droplets in case of moist air.

The generation of condensate properties is in the same manner as discussed. The graphical results for $\theta=8.5^\circ$ are not shown here for brevity. However, the value of

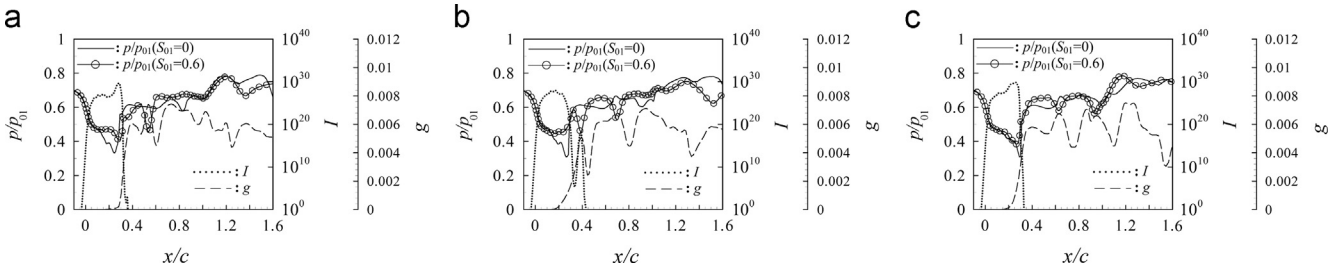

Figure 14 Distributions of static pressure (p/p_{01}), nucleation rate (I) and condensate mass fraction (g) along line A-A' around a plate ($\theta=3.2^\circ$). (a) $t=0.333T$ (ms), (b) $t=0.667T$ (ms), and (c) $t=1.000T$ (ms).

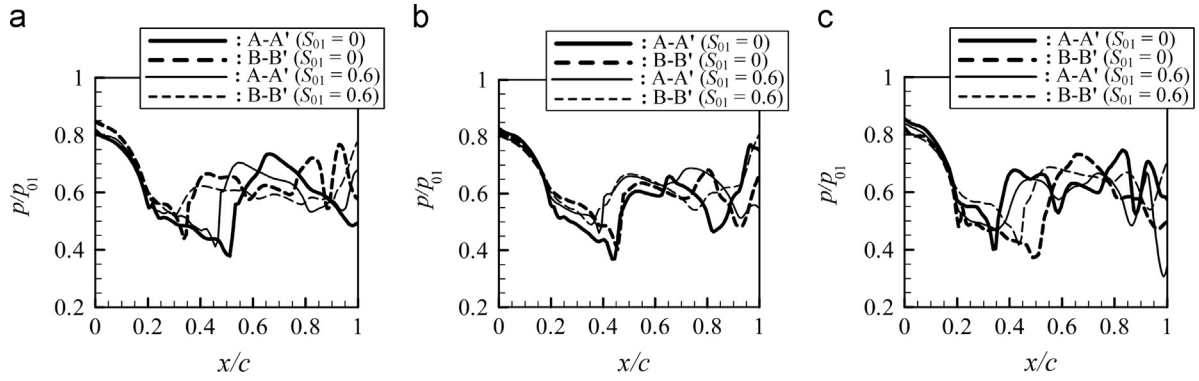

Figure 15 Distribution of static pressure (p/p_{01}) around a prototype butterfly valve ($\theta=0^\circ$). (a) $t=0.333T$ (ms), (b) $t=0.667T$ (ms), and (c) $t=1.000T$ (ms).

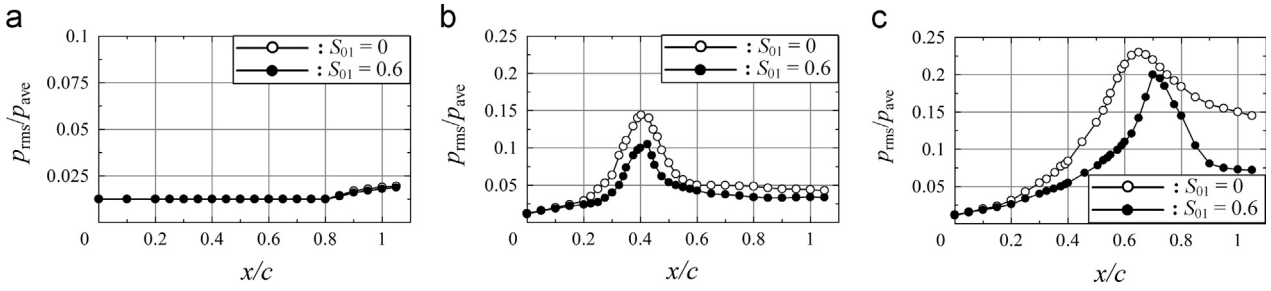

Figure 16 Distribution of root mean square (RMS) value of pressure oscillation around a plate. (a) $\theta=0^\circ$, (b) $\theta=3.2^\circ$, and (c) $\theta=8.5^\circ$.

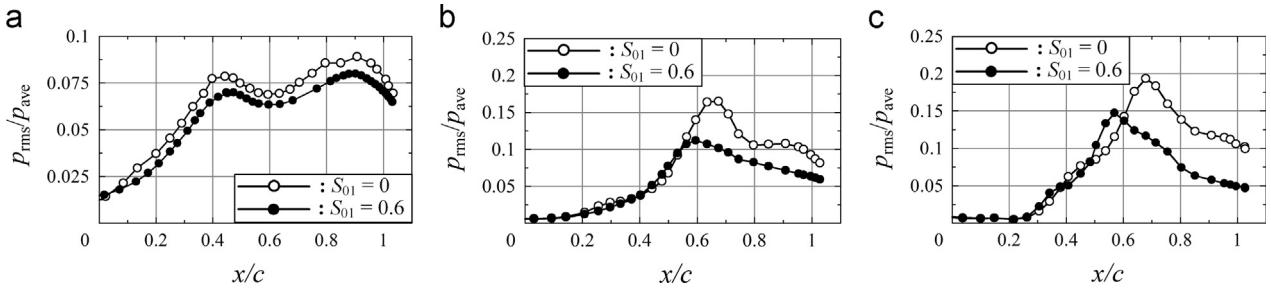

Figure 17 Distribution of root mean square (RMS) value of pressure oscillation around a prototype butterfly valve. (a) $\theta=0^\circ$, (b) $\theta=3.2^\circ$, and (c) $\theta=8.5^\circ$.

condensate mass fraction is highest for $\theta=8.5^\circ$ compared with $\theta=0^\circ$ and $\theta=3.2^\circ$, and the maximum is about 0.01. This is due to maximum reduction of cross section area at the leading edge in the upper passage at this condition.

Figure 15 shows the distributions of static pressure p/p_{01} around a prototype butterfly valve along the lines A-A′ and B-B′ during one cycle of flow oscillation T for $\theta=0^\circ$. In case of $S_{01}=0$, shock waves along line A-A′ are observed to

develop from $x/c \approx 0.5$ and travel toward the leading edge during the cycle. Along line B-B′, shock waves are moving from leading to trailing edge. Thus, shock waves are oscillating alternatively in between the upper and lower passages during the cycle. In case of $S_{01}=0.6$, the maximum degree of expansion in the flow is reduced and thus the strength of shock wave becomes weak compared to the case of $S_{01}=0$. Furthermore, the distribution of p/p_{01} indicates that the strength of shock wave gradually decreases when shock wave is moving towards the leading edge of the valve in both the cases. In addition, the generations of condensate properties are in the same manner as discussed in case of plate. Other angles of attack ($\theta=3.2^\circ$ and 8.5°) showed the similar flow phenomena as discussed for $\theta=0^\circ$ (Figure 15).

Now, the aerodynamic instability induced by the unsteady shock waves around the plate will be discussed using the parameter - root mean square (RMS) value of pressure oscillation. Figure 16 shows the distribution of RMS value of pressure oscillation p_{rms}/p_{ave} (p_{rms}: RMS of pressure oscillation; p_{ave}: average of pressure oscillation) around upper passage of the plate for $\theta=0^\circ$, 3.2° and 8.5° in cases without and with spontaneous condensation. At $\theta=0^\circ$ (Figure 16(a)), the compression waves at the trailing edge of the plate causes the RMS values to increase to about 0.02. Since there is no condensate mass fraction at these locations, RMS values are almost the same for $S_{01}=0$ and $S_{01}=0.6$. In case of $\theta=3.2^\circ$ (Figure 16(b)), the RMS values are higher than $\theta=0^\circ$ (Figure 16(a)) at all axial positions. A peak is observed at $x/c \approx 0.4$ and the value is about 0.15 for $S_{01}=0$. For $S_{01}=0.6$, reduction of RMS values are found in all axial positions and the peak value is about 0.11. For $\theta=8.5^\circ$ (Figure 16(c)), the peak RMS values are 0.23 and 0.2 in cases of $S_{01}=0$ and 0.6, respectively.

Results in case of prototype butterfly valve is shown in Figure 17. At $\theta=0^\circ$ (Figure 17(a)), two peaks are observed in both the cases of $S_{01}=0$ and $S_{01}=0.6$. However, the second one is more dominating than the first and located at about $x/c=0.9$. In all axial locations, the RMS values are smaller in case of $S_{01}=0.6$ to those of $S_{01}=0$. The peak p_{rms}/p_{ave} values are 0.09 and 0.08 for $S_{01}=0$ and $S_{01}=0.6$, respectively. For $\theta=3.2^\circ$ (Figure 17(b)), the RMS values are comparable up to $x/c=0.55$ in both the cases of $S_{01}=0$ and 0.6. After that the RMS values are reduced in case of $S_{01}=0.6$. The peak RMS values are 0.17 and 0.11 for $S_{01}=0$ and $S_{01}=0.6$, respectively. However, in case of $S_{01}=0.6$, peak RMS position is moved upstream ($x/c=0.58$) to that of $S_{01}=0$ ($x/c=0.68$). Reduction in RMS values and upstream shift of peak RMS position in case of spontaneous condensation are also observed for $\theta=8.5^\circ$ shown in Figure 17(c).

The aerodynamic torque is primarily a function of valve angle, the operating pressure ratio and valve geometry. A qualitative discussion of local moment distributions on the plate surface provides insight into the torque characteristics. Figure 18 shows distributions of local moment for $\theta=0^\circ$, 3.2° and 8.5° during one cycle of flow oscillation in case of no condensation ($S_{01}=0$) for a plate. The dimensionless local moment on the plate is defined here as the local pressure difference across the disk multiplied by the moment arm about the axis of rotation divided by the product of upstream stagnation pressure (p_{01}) and test section height (H) This definition is the same as one defined in [17]. The axis of rotation is at point A ($x/c=0.5$, $y/c=0$). P_u and P_l are the pressures on upper and lower surfaces of the plate, respectively and x' is the moment arm. Sign convention for moment is shown in these figures. For $\theta=0^\circ$ (Figure 18(a)), local moments are zero except the range close to the leading and trailing edges of the plate. Flow separation and

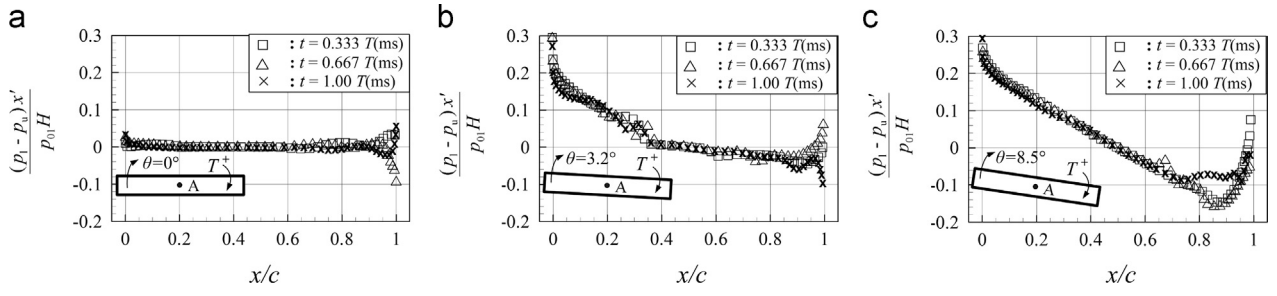

Figure 18 Local moment distribution for a plate ($S_{01}=0$). (a) $\theta=0^\circ$, (b) $\theta=3.2^\circ$, and (c) $\theta=8.5^\circ$.

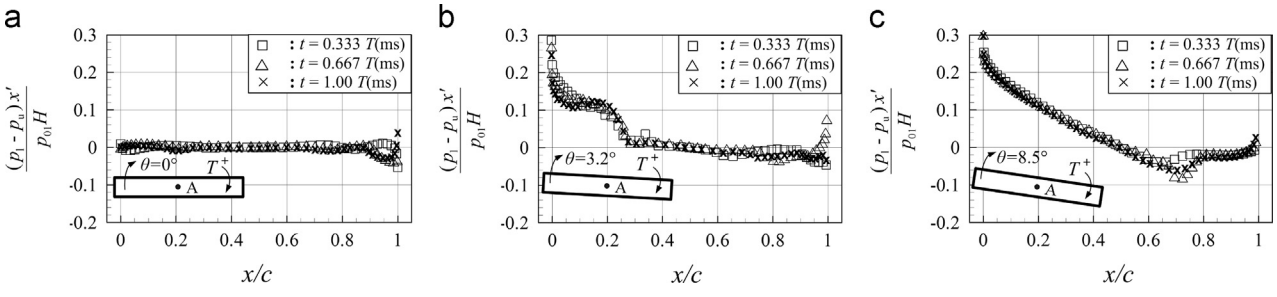

Figure 19 Local moment distribution for a plate ($S_{01}=0.60$). (a) $\theta=0^\circ$, (b) $\theta=3.2^\circ$, and (c) $\theta=8.5^\circ$.

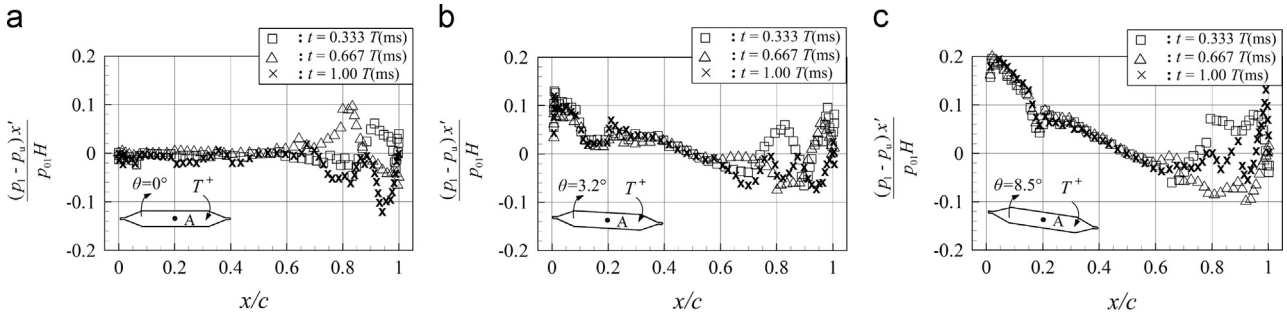

Figure 20 Local moment distribution for a prototype butterfly valve ($S_{01}=0$). (a) $\theta=0^\circ$, (b) $\theta=3.2^\circ$, and (c) $\theta=8.5^\circ$.

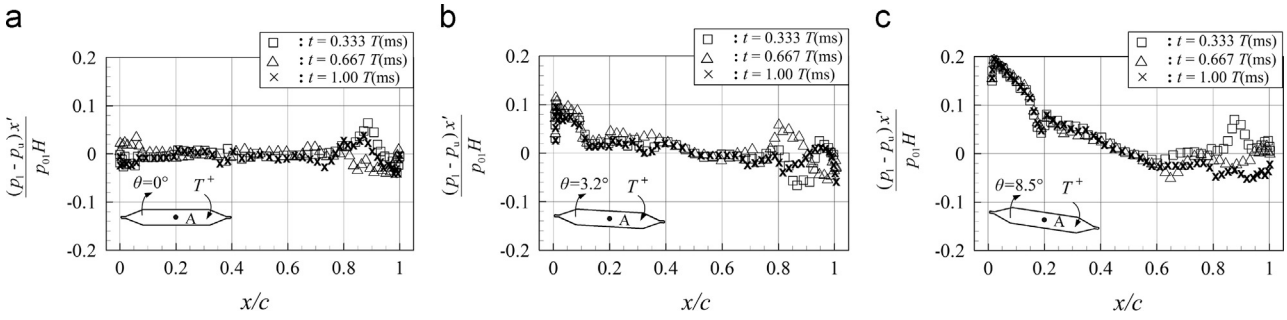

Figure 21 Local moment distribution for a prototype butterfly valve ($S_{01}=0.60$). (a) $\theta=0^\circ$, (b) $\theta=3.2^\circ$, and (c) $\theta=8.5^\circ$.

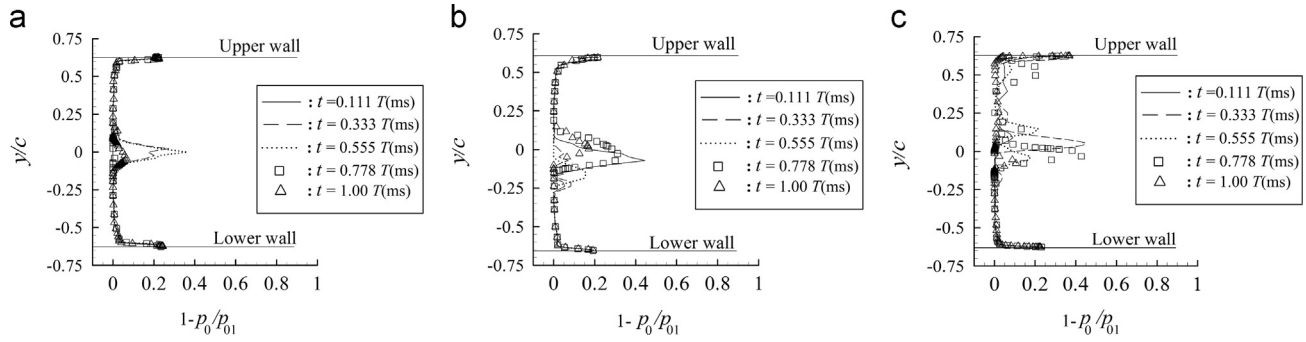

Figure 22 Distribution of total pressure losses during one cycle of flow oscillation for a plate ($x/c=1.5$, $S_{01}=0$). (a) $\theta=0^\circ$, (b) $\theta=3.2^\circ$, and (c) $\theta=8.5^\circ$.

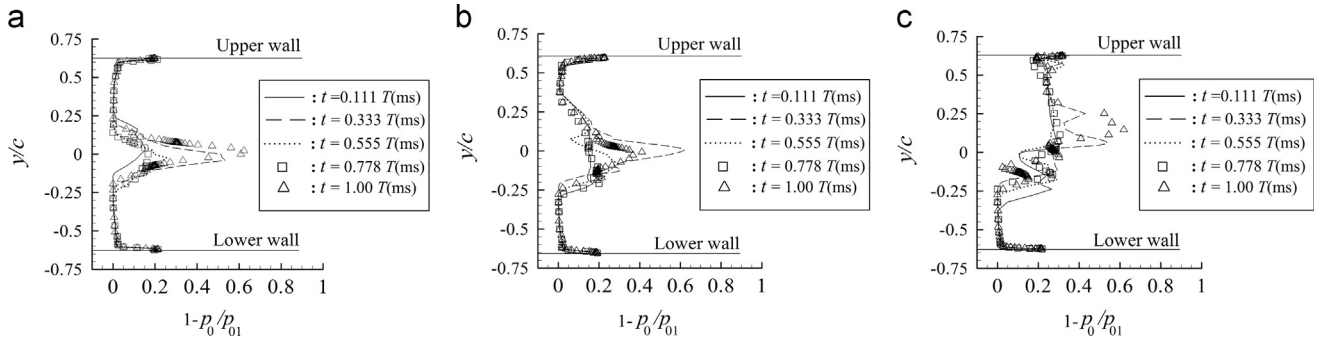

Figure 23 Distribution of total pressure losses during one cycle of flow oscillation for a plate ($x/c=1.5$, $S_{01}=0.6$). (a) $\theta=0^\circ$, (b) $\theta=3.2^\circ$, and (c) $\theta=8.5^\circ$.

compressive waves are responsible for non zero local moment distributions around leading and trailing edges, respectively. For $\theta=3.2^\circ$ (Figure 18(b)), upstream of the midchord, forces result in relatively large positive closing moments at locations with large moment arm. This is due to relatively large pressure differences induced by rapid increase in pressure by shock wave at upper surface at $x/c<0.5$. Downstream of the midchord, $x/c>0.5$, the pressure difference

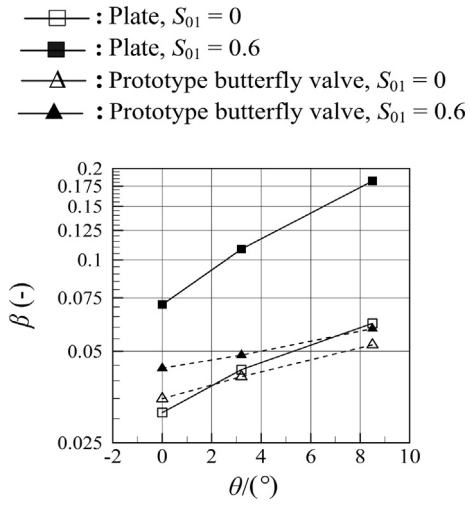

Figure 24 Time averaged integrated total pressure loss (β) for two different valve disk shapes ($x/c=1.5$).

across the plate is small and thus the moments are relatively small. For $\theta=8.5^\circ$ (Figure 18(c)), large separation at the leading edge and thus low pressure recirculation region at the plate upper surface cause very large positive closing moments in the range of $x/c<0.5$. After $x/c>0.5$, shock waves on plate upper surface result in negative moments. The large negative moments are observed in the range of $0.8<x/c<0.95$. Asymmetric moment distributions about the axis of rotation are clearly observed for angles of attack $\theta=3.2^\circ$ and 8.5° compared with the case of $\theta=0^\circ$. Local moment distributions for the case with spontaneous condensation are shown in Figure 19 ($S_{01}=0.6$). For $\theta=0^\circ$ (Figure 19(a)), it is observed that moment values are reduced to some extent in the range close the trailing edge compared with the case of no condensation (Figure 18(a)). In case of plate with angle of attack, $\theta=3.2^\circ$ (Figure 19(b)), the positive closing moments are observed up to $x/c\approx0.25$, which is smaller compared with result ($x/c\approx0.35$) in Figure 19(b). Above $x/c\approx0.25$, the moments are almost zero except the range close to the trailing edge. For $\theta=8.5^\circ$ (Figure 19(c)), the moment distributions are comparable to those of case of no condensation (Figure 18(c)) up to $x/c<0.5$. Downstream of midchord, $x/c>0.5$, relatively small pressure difference across the plate and thus smaller negative moment values is attributed to the reduction of shock strength in the plate upper region.

Results for the case of a prototype butterfly valve are shown in Figure 20. For $\theta=0^\circ$ (Figure 20(a)), local moments are close to zero upto the midchord, $x/c=0.5$. At $x/c>0.5$, large positive and negative moments are observed alternatively during the cycle. This is due to the alternative shock oscillation in between upper and lower passage as discussed before. For $\theta=3.2^\circ$ (Figure 20(b)), upstream of the midchord, the large positive closing moments are in the same manner shown in Figure 18(b). Downstream of the midchord, $x/c>0.5$, the appearance of shock waves causes the large moment distribution. At the trailing edge, though the pressure differences are small, large moment arm also makes the moment values higher. For $\theta=8.5^\circ$ (Figure 20(c)), shock waves and shock induced oscillation on valve upper surface result in large moments. The large moments are observed in the range of $0.75<x/c<1.0$. With the occurrences of spontaneous condensation, the local moments are reduced for all angles of attack compared to dry air shown in Figure 21.

Figure 22 shows distributions of total pressure loss ($1-p_0/p_{01}$) (p_0: local total pressure) for plate along y-direction at the position of $x/c=1.5$ in case without spontaneous condensation one cycle. However, unsteadiness of total pressure losses increases with an increase of angle of attack. The maximums of total pressure loss values for $\theta=0^\circ$, 3.2° and 8.5° are observed in the range of $y/c=-0.15\sim0.15$, $-0.3\sim0.2$ and $-0.3\sim0.6$, respectively. For $\theta=8.5^\circ$ (Figure 22(c)), much variation of total pressure losses are observed in the region close to the upper wall compared with other cases. This is due to the boundary layer separation induced by shock wave at the upper wall. Total pressure losses in case with spontaneous condensation along y-direction during one cycle of flow oscillation are shown in Figure 23 ($x/c=1.5$, $S_{01}=0.6$). It is found from this figure that values of total pressure loss become larger compared with case of dry air in Figure 22. Moreover, y-range of occurrence of total pressure losses is increased for all angles of attack compared to Figure 22. The increase of total pressure loss is considered to be due to the generation of condensate droplets (induced by spontaneous condensation) and the associated heat transfer to the flow field. This heat transfer enhances the entropy of the transonic flow field in moist air case and the corresponding total pressure loss compared to no condensation in case of dry air flows. Similar results are also found for a prototype butterfly valve and not shown here for brevity.

Total pressure losses were integrated from the lower wall to the upper wall at $x/c=1.5$ and the time averaged value β is shown for a plate and a prototype butterfly valve at each angles of attack in Figure 24. With an increase of angle of attack, β increases in cases without and with spontaneous condensation for both the valve disk shapes. For plate, with the occurrence of condensation, values of β for $\theta=0^\circ$, 3.2° and 8.5° increase approximately by 125%, 150% and 200% compared to the case of no condensation, respectively. However, in case of a prototype butterfly valve, β increases approximately 25%, 18% and 15% with condensation ($S_{01}=0.6$) for $\theta=0^\circ$, 3.2° and 8.5°, respectively.

Further, it could be observed that the total pressure loss for the butterfly valve is significantly less than that for the plate. The geometric shape of the plate with sharp leading and trailing edges causes more viscous separation compared to prototype valve with round edges. Viscous separation (together with other sources) also contributes to the total pressure loss. Thus, the difference in total pressure loss is obviously due to the difference in viscous separation while comparing the transonic flows over a plate and a butterfly valve.

Flow oscillation frequency is measured in the wake region at $x/c=1.5$, $y/c=0$. The dominant frequencies are shown in Table 1 for both the rectangular plate profile and a prototype butterfly valve in cases of no condensation ($S_{01}=0$) and with condensation ($S_{01}=0.6$). The frequency values are smaller for a prototype butterfly valve to those of

Table 1 Dominant frequency of flow oscillation in kHz measured at $x/c=1.5$, $y/c=0$.

	Plate			Prototype butterfly valve		
S_{01} \ θ	0°	3.2°	8.5°	0°	3.2°	8.5°
0	17.05	15.71	6.16	3.08	3.48	5.22
0.6	07.03	7.59	3.61	1.60	2.08	2.90

a flat rectangular plate profile for both the cases of $S_{01}=0$ and $S_{01}=0.6$. Moreover, the frequencies are reduced significantly with the occurrences of spontaneous condensation compared with the case of no condensation for both the valve shapes Reduction of dominant frequency is considered to be due to the decrease of turbulent fluctuation energy by the relaxation process of condensation and evaporation of vapor molecules on small droplet surfaces, and the interaction of boundary layer with shock wave becomes weak due to reduction of Mach number upstream of the shock wave.

4. Conclusions

A computational and experimental simulation was carried out to investigate the effect of spontaneous condensation on the aerodynamic characteristics of butterfly valves in transonic flow field. The Mach number upstream of the valve was 0.6. Two valve disk shapes have been studied in the present study: a flat rectangular plate and a mid-plane cross-section of a prototype butterfly valve. Results obtained are as follows:

- With the occurrences of spontaneous condensation, the shock strength was reduced in both the valves and for all angles of attack studied here ($\theta=0°$, 3.2° and 8.5°).
- In case of rectangular plate, condensate nuclei and droplets were observed in the wake region for $\theta=0°$. For $\theta=3.2°$ and 8.5°, spontaneous condensation was induced around the plate upper passage including downstream range. However, for prototype butterfly valve, the condensate properties are developed in between upper and lower passages up to downstream range.
- The flow field aerodynamic instabilities such as root mean square (RMS) of pressure oscillation is reduced significantly in moist air with those without spontaneous condensation (dry air) for both shapes of the valves.
- Local moments on the rectangular plate and a prototype butterfly valve were reduced in case with spontaneous condensation which is considered to be beneficial in the torque requirement in case of on/off applications for flow control devices.
- Total pressure loss increased in case of moist air.
- In the wake region, the vortex shedding frequency was reduced with spontaneous condensation.
- Furthermore, the disk shape of a prototype butterfly valve showed better aerodynamic performance in respect of total pressure loss and vortex shedding frequency to that of a flat rectangular plate profile.

References

[1] I. Fejtek, G. Waller, R. Wong, Computational study of the flowfield of an aircraft outflow valve, in: Proceedings of 23rd Aerodynamic Conference, Toronto, Ontario, Canada, AIAA 2005-4843, 2005.
[2] A.D. Henderson, J.E. Sargison, G.J. Walker, J. Haynes, A numerical study of the flow through a safety butterfly valve in a hydro-electric power scheme, in: Proceedings of 16th Australasian Fluid Mechanics Conference, Australia, 2007, pp. 1116–1122.
[3] F. Danbon, C. Solliec, Aerodynamic torque of a butterfly valve- influence of an elbow on the time-mean and instantaneous aerodynamic torque, ASME Journal of Fluids Engineering 122 (3) (2000) 337–344.
[4] Z. Leutwyler, C. Dalton, A CFD study of the flow field, resultant force, and aerodynamic torque on a symmetric disk butterfly valve in a compressible fluid, ASME Journal of Pressure Vessel Technology 130 (2) (2008) 021302-1-021302-10.
[5] Z. Leutwyler, C. Dalton, A computational study of torque and forces due to compressible flow on a butterfly valve in mid-stroke position, ASME Journal of Fluids Engineering 128 (5) (2006) 1074–1082.
[6] A.L. Addy, M.J. Morris, J.C. Dutton, An investigation of compressible flow characteristics of butterfly valves, ASME Journal of Fluids Engineering 107 (2) (1985) 512–517.
[7] M.J. Morris, J.C. Dutton, Compressible flowfield characteristics of butterfly valves, ASME Journal of Fluids Engineering 111 (4) (1989) 400–407.
[8] Z. Rusak, J.C. Lee, Transonic flow of moist air around a thin airfoil with non-equilibrium and homogeneous condensation, Journal of Fluid Mechanics 403 (2000) 173–199.
[9] X. Luo, G. Lamanna, A.P.C. Holten, M.E.H. van Dongen, Effects of homogeneous condensation in compressible flows: Ludwieg-tube experiments and simulations, Journal of Fluid Mechanics 572 (2007) 339–366.
[10] J.P. Sislian, Condensation of water vapor with or without a carrier gas in a shock tube, UTIAS Report, No.201, 1975.
[11] U.C. Goldberg, Towards a pointwise turbulence model for wall-bounded and free shear flows, ASME Journal of Fluids Engineering 116 (1) (1994) 72–76.
[12] M.Heiler, Instationäre Phänomene in Homogen/Heterogen Kondensierenden Düsen- und Turbinenströmungen, Ph.D Dissertation, Universität Karlsruhe (TH) Germany, 1999.
[13] H.C. Yee, A class of high-resolution explicit and implicit shock capturing methods, NASA TM-89464, 1989.
[14] A.B.M. Toufique Hasan, S. Matsuo, T. Setoguchi, H.D. Kim, Transonic moist air flow around a circular arc blade with bump, Journal of Thermal Science 18 (4) (2009) 325–331.
[15] A.B.M. Toufique Hasan, S. Matsuo, T. Setoguchi, A.K.M.S. Islam, Effects of condensing moist air on shock induced

oscillation around an airfoil in transonic internal flows, International Journal of Mechanical Sciences 54 (1) (2012) 249–259.

[16] J.C. Huang, R.I. Gault, E. Benard, S. Raghunathan, Effect of humidity on transonic flow, Journal of Aircraft 45 (6) (2008) 2092–2100.

[17] M.J. Morris, J.C. Dutton, Aerodynamic torque characteristics of butterfly valves in compressible Flow, ASME Journal of Fluids Engineering 111 (4) (1989) 392–399.